Hindawi
Journal of Nanomaterials
Volume 2021, Article ID 9961663, 10 pages
https://doi.org/10.1155/2021/9961663

Research Article

Electrospun Nanofibers with High Specific Surface Area to Prepare Modified Electrodes for Electrochemiluminescence Detection of Azithromycin

Hao Cheng,[1,2] **Xuenuan Li**,[1] **Tianhao Li**,[1] **Danfeng Qin**,[1] **Tingfan Tang**,[1] **Yanqing Li**,[1] **and Guixiang Wang**[3]

[1]*Guangxi Key Laboratory of Green Processing of Sugar Resources, College of Biological and Chemical Engineering, Guangxi University of Science and Technology, Liuzhou, 545006 Guangxi, China*
[2]*Province and Ministry Co-Sponsored Collaborative Innovation Center of Sugarcane and Sugar Industry, Nanning, 530004 Guangxi, China*
[3]*College of Chemistry and Chemical Engineering, Taishan College, Tai'an 271021, Shandong, China*

Correspondence should be addressed to Yanqing Li; liyanqing@gxust.edu.cn and Guixiang Wang; wangguixiang@tsu.edu.cn

Received 1 April 2021; Accepted 7 June 2021; Published 19 July 2021

Academic Editor: Jim Low

Polyacrylonitrile (PAN) and $(CH_3COO)_2Zn$ were used as raw materials, and carbon nanofibers (CNFs) with high specific surface area were successfully prepared by an electrospinning method. A new method of electrochemiluminescence detection of azithromycin was established by modifying the glassy carbon electrode (GCE). Under the optimal conditions, the electrochemical behavior and electrochemiluminescence behavior of the $Ru(bpy)_3^{2+}$-AZM system on the modified electrode were investigated. Owing to the large specific area, more active sites, and promotion of electron transfer, the sensor exhibits high electrocatalytic activity, high sensitivity, a good linear relationship ranging from 8.0×10^{-8} to 1.0×10^{-4} mol/L, and a low detection limit (6.52×10^{-8} mol/L). In addition, the good recoveries indicate that the sensor was a promising device for the detection of azithromycin in real samples.

1. Introduction

Azithromycin (AZM), as a macrolide antibiotic, has a broad-spectrum antibacterial activity. It mainly inhibits the process of bacterial transpeptidation to inhibit the synthesis of proteins in bacteria, thereby acting as an antibacterial agent. It has the characteristics of long half-life and high tissue drug concentration. It can be used clinically to treat various infections such as urinary system infection and respiratory system infection. However, when the accumulation of AZM in the body exceeds a certain amount, it will bring a series of side effects such as cardiovascular death, gastrointestinal and nervous system damage, and anaphylactic shock [1, 2].

At present, the main methods for determining azithromycin are high-performance liquid chromatography (HPLC) [3], spectrophotometry [4], high-performance liquid phase-mass spectrometry [5], electrochemical method [6], ultraviolet spectrophotometry [7], and other methods. But some of them have the limitations of expensive equipment and cumbersome operation. Therefore, it is necessary to establish a fast and accurate detection method.

CNF material has attracted the attention of researchers as electrode modification materials due to its stable chemical properties and good electrical conductivity [8]. However, In terms of the high-sensitivity requirements [9] of analytical detection methods, it nedds CNFs with higher specific surface area [10] which are preparedd to meet this demand. Combining the advantages of electrochemistry and chemiluminescence, electrochemiluminescence has the characteristics of high sensitivity and fast detection speed, which is favored by researchers [11–14].

In this study, the prepared CNF modified GCE with higher specific surface area was used as the working electrode to study the electrochemiluminescence behavior of azithromycin-$Ru(bpy)_3^{2+}$ system, and the influence of different experimental conditions on the luminescence behavior of AZM was investigated. Based on this, a new method for the determination of AZM was established.

2. Experiments

2.1. Materials. A standard stock solution with a concentration of 1.5×10^{-3} mol/L of AZM was prepared by dissolving AZM (Shanghai Yuanye Biological Technology Co., Ltd.) into ultrapure water and stored in a refrigerator. A stock solution of $Ru(bpy)_3^{2+}$ was prepared by dissolving $Ru(bpy)_3Cl_2{\cdot}6H_2O$ in ultrapure water. Polyacrylonitrile (PAN, molecular weight: 85,000 g/mol, Sigma-Aldrich Co., Ltd. Shanghai, China) was used as the carbon source for the nanofibers. N, N-Dimethylformamide (DMF), isopropanol, and Nafion solution (5 wt.%) were purchased from Sigma-Aldrich (Shanghai, China). All the chemicals used in the experiments were of analytical grade, and ultrapure water was used. A 0.1 M borate buffer solution (pH = 8.5) was prepared by mixing a 0.1 M NaH_2PO_4 solution and a Na_2HPO_4 solution. Zinc acetate ($(CH_3COO)_2Zn$) was purchased from Shanghai Yuanye Biotechnology Technology Co., Ltd.

2.2. Instruments. Field-emission scanning electron microscope (FE-SEM, Carl Zeiss, Germany) was used to observe the external morphology of the synthesized materials. An X-ray photoelectron spectroscope (XPS, Kratos Analytical Ltd., UK) was used to determine the elemental composition of the surface layer of materials. A laser confocal Raman microspectroscope (Raman, XploRA PLUS, Horiba) was used to measure the Raman spectra of the materials.

2.3. Synthesis of CNFs-1/CNFs-2. 1.2 g PAN and 1.0 g $(CH_3COO)_2Zn$ were added to DMF and stirred at room temperature for 12 h to obtain a spinning precursor solution. The parameter setting of the electrospinning device is as follows. Electrostatic spinning voltage was 18 kV. The distance between the needle tip and the collector was 10 cm. The flow rate was 2.0 mL·h^{-1}. The speed of the spinning collector was 180 r·min^{-1}. After drying in a vacuum for 12 h, the composite nanofibers were calcinated in N_2 at 800°C with a heating rate of 5°C/min. After carbonization, it was naturally cooled to room temperature and the material was placed in hydrochloric acid to etch ZnO residue. Then, the solid was rinsed with deionized water to neutrality and dried at 80°C. Finally, high specific surface area of CNFs was obtained, marked as CNFs-2. For comparison experiments, unmodified CNFs, labeled as CNFs-1, were prepared with the same spinning parameters and carbonization conditions.

2.4. Fabrication of CNFs-1/GCE and CNFs-2/GCE. Prior to the fabrication of the final electrode, the GCE was polished until it became a mirror-like surface using fine emery papers and 0.3 μm and 0.05 μm alumina slurry. Afterwards, the GCE was cleaned ultrasonically using deionized water and ethanol alternatively and then dried in a N_2 atmosphere. Subsequently, 1.5 mg of CNFs-1 were dispersed via sonication in isopropanol-H_2O (1 : 4,*v*/*v*) to produce a homogeneous and stable suspension. Then, 3 μL of the prepared suspension was pipetted onto to the polished surface of the GCE, followed by drying at room temperature. Through this process, CNFs-1/GCE was obtained. The CNFs-2 modified electrode (CNFs-2/GCE) was prepared in the same way.

2.5. Electrochemical and Electrochemiluminescence Measurements. In this study, all electrochemical (EC) and electrochemiluminescence (ECL) measurements were performed using a MPI-E electrogenerated chemiluminescence analyzer (Xi'an Remex (Ruimai) Analysis Instruments Co., Ltd., Xi'an, China) with a three-electrode cell. The working electrode was bare GCE or modified GCE (Φ = 3 mm). The counter electrode was a Pt wire. And the reference electrode was made of Ag/AgCl. Cyclic voltammetry (CV) measurements were carried out to determine the EC and ECL properties of AZM. The sample was put in a phosphate buffer solution (0.1 M, pH = 8.5) under optimal conditions. A high negative voltage of -800 V was applied to the photomultiplier. The scan rate was 100 mV/s, and the concentration of $Ru(bpy)_3^{2+}$ was 4×10^{-4} M.

3. Results and Discussion

3.1. Drug Substance Characterization. Figure 1 shows the SEM images of CNFs-1 and CNFs-2. It can be seen from Figures 1(a) and 1(c) that the material is indeed continuous and uniform fibrous, and the addition of $(CH_3COO)_2Zn$ does not change the overall morphology of the material. It can be seen from Figure 1(b) that the surface of the fibers without $(CH_3COO)_2Zn$ is relatively smooth, and after, the specific surface area of the fiber is improved. As shown in Figure 1(d), the surface of the fibers becomes rougher and there are a lot of pits, which shows that the addition and elution of $(CH_3COO)_2Zn$ does have a certain effect on the surface of fibers.

The element composition and chemical bond structure of the CNFs-2 material were further characterized and analyzed by XPS, and the results are shown in Figure 2. The analysis results show that the material is composed of C, N, and O and the contents of elements are 88.49%, 4.47%, and 7.04%, respectively. It can be seen from Figure 2(b) that C1s exists in CNF-2 in three forms: sp2-C (284.5 eV), sp3-C (285.2 eV), and C=O/C-N (287.9 eV) [15]. As shown in Figure 2(c), N1s is fitted to three bands, namely, pyridine N at 398.3 eV, pyrrole N at 399.8 eV, and graphite N at 400.8 eV. Among them, pyridine N, pyrrole N, and graphite N account for 45.92%, 30.49%, and 23.59%, respectively. A higher proportion of pyridine N is found in CNFs-2. It can improve conductivity and accelerate ion transmission and diffusion [16]. Figure 2(d) is the analytical spectrum of O1s. O1s has two analytical peaks of C=O (531.5 eV) and CO (532.4 eV). The presence of higher polar oxygen and nitrogen-containing groups can improve the hydrophilicity and electroactive specific surface area of CNFs-2, which is beneficial to improve the performance of CNFs-2/GCE [17–19].

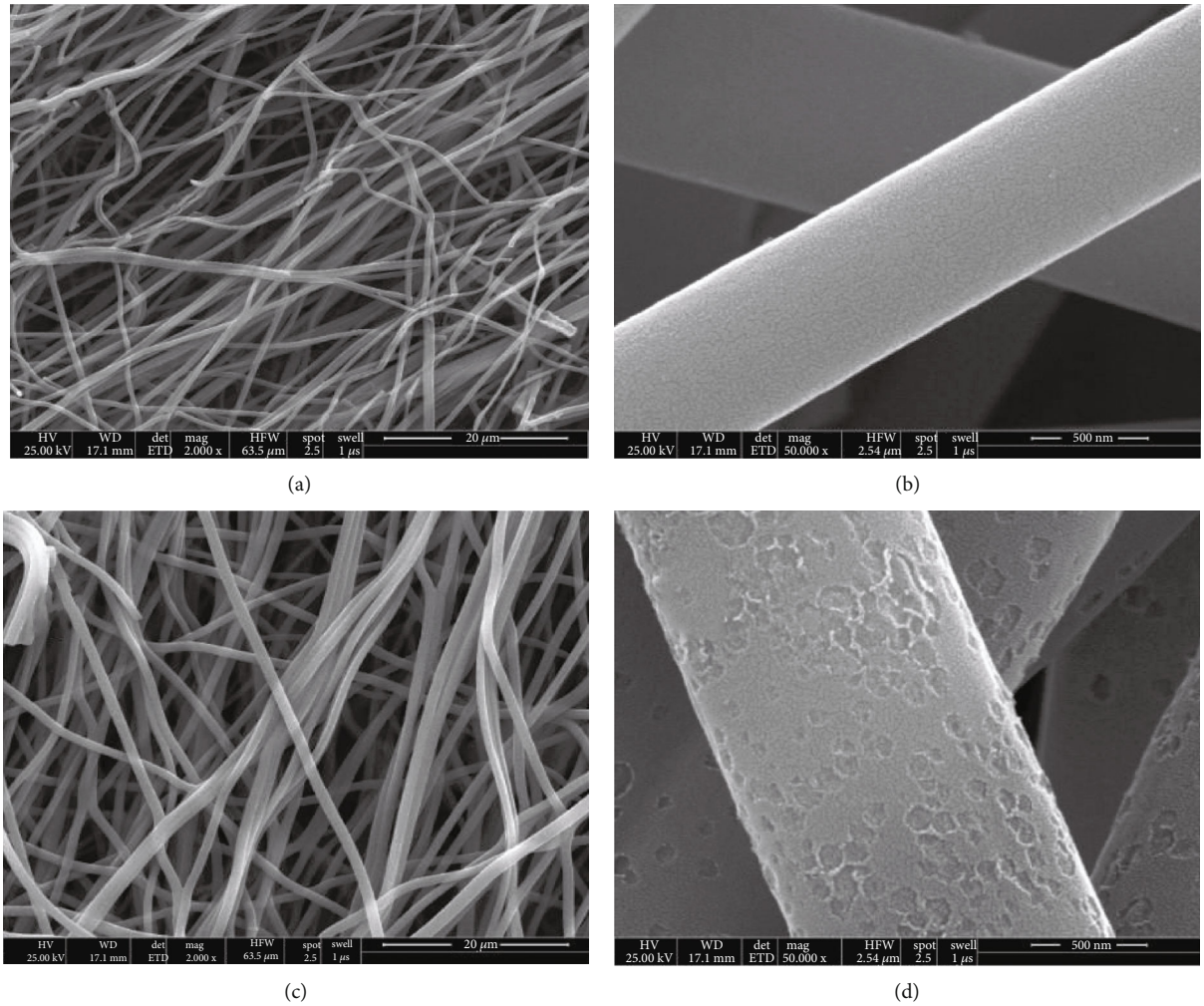

Figure 1: (a, b) The SEM images of CNFs-1; (c, d) the SEM images of CNFs-2.

Figure 3(a) is the XRD analysis result of the sample. It can be seen that a strong and broad diffraction peak is found at $2\theta = 25.5^{\circ}$, while a weak and narrow peak is observed at $2\theta = 43^{\circ}$. It indicates that CNF-2 is a disordered carbon material [20]. Raman spectroscopy is used to conduct an in-depth analysis of the disorder of the material. There are two typical characteristic peaks at $1360\,cm^{-1}$ and $1601\,cm^{-1}$ in Figure 3(b), namely, the D band and the G band [21, 22]. The I_D/I_G of CNFs-2 is 1.03, indicating that CNFs-2 has a high degree of disorder [23], which is consistent with the results of XRD. The pore structure and specific surface area of CNFs-2 were characterized and analyzed by the N_2 adsorption-desorption method. The results are illustrated in Figure 3. As shown in Figure 3(c), the adsorption curve and desorption curve in the isotherm of CNFs-2 are inconsistent, and there are H1 hysteresis loops. It belongs to type IV and has the characteristics of layered pores, which proves that there is a very small amount of mesoporous structure. Figure 3(d) shows the pore size distribution curve. It can be seen from the figure that the pore size of CNFs-2 is mainly concentrated at 35 nm, indicating that a small amount of mesopores exist, which is consistent with the characterization results of the N_2 adsorption-desorption curve. In addition, the specific surface area of CNFs-1 is $18\,m^2 \cdot g^{-1}$ and the total pore volume is $0.01\,cm^3 \cdot g^{-1}$, while the specific surface area of CNFs-2 is $543\,m^2 \cdot g^{-1}$ and the total pore volume is $0.19\,cm^3 \cdot g^{-1}$. Its specific surface area is 18 times that of CNFs-1. Importantly, a higher specific surface area can provide more reactive sites during the detection process, thereby improving the performance of the material.

3.2. EC and ECL Behaviors of AZM

3.2.1. EC and ECL Behaviors of $Ru(bpy)_3^{2+}$, AZM, and $Ru(bpy)_3^{2+}$-AZM Systems. Figure 4 shows the EC behavior and ECL behavior of $Ru(bpy)_3^{2+}$ and $Ru(bpy)_3^{2+}$-AZM on the modified electrode. It can be seen from Figure 4(a) that, after adding AZM to $Ru(bpy)_3^{2+}$, the oxidation peak current significantly increases and the reduction peak current decreases, indicating that AZM can promote the electrochemical reaction of $Ru(bpy)_3^{2+}$, thus making the electrochemical response change. As shown in Figure 4(b), AZM has no obvious luminescence, and the luminescence intensity of $Ru(bpy)_3^{2+}$ is also very weak, indicating that the

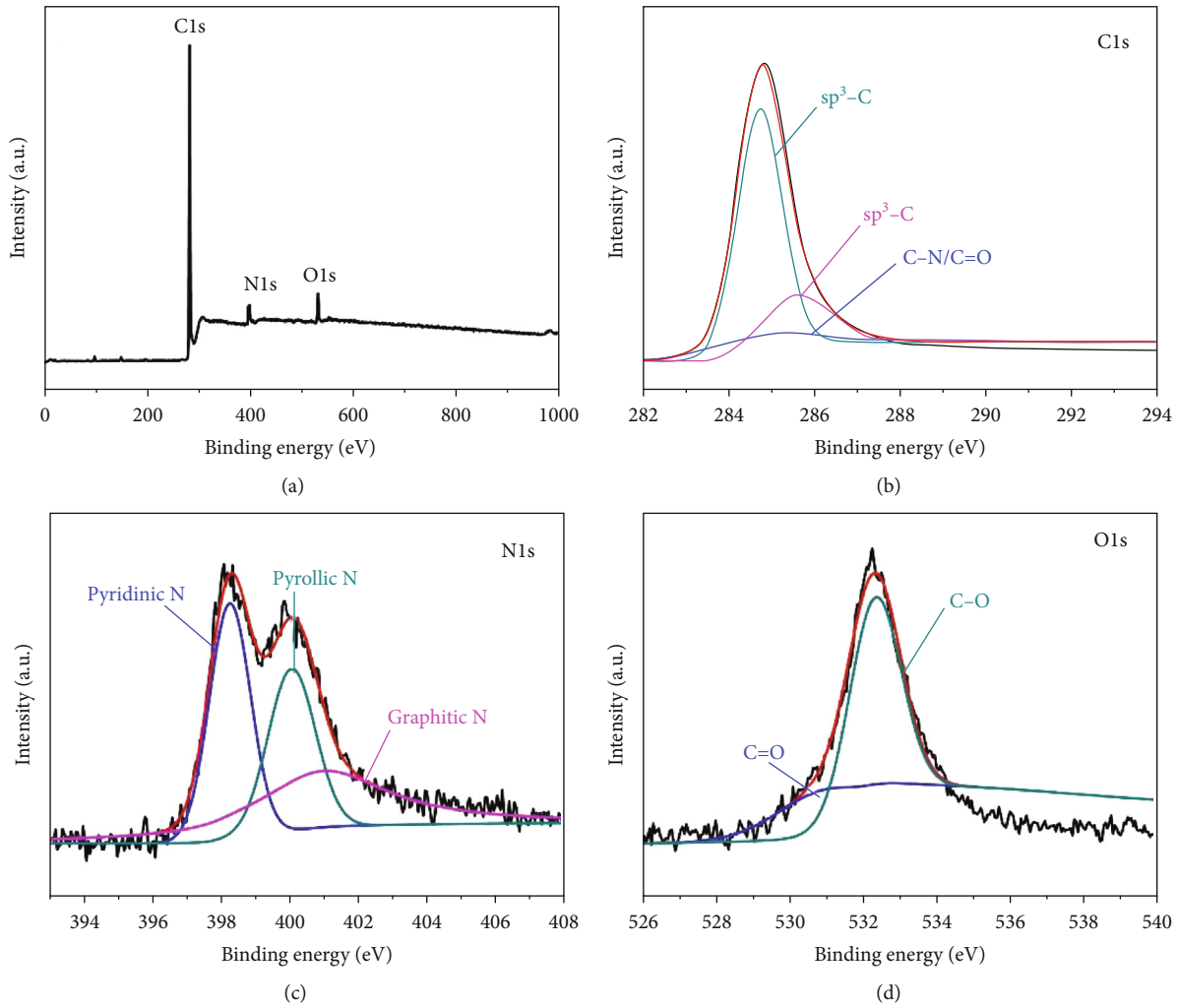

Figure 2: XPS survey spectra (a), high-resolution XPS spectra of C1s peak (b), N1s peak (c), and O1s (d) of CNFs-2.

background signal is low. When AZM was added to $Ru(bpy)_3^{2+}$, the luminescence intensity was significantly enhanced, indicating that AZM has a sensitizing effect on $Ru(bpy)_3^{2+}$.

3.2.2. EC and ECL Behaviors of $Ru(bpy)_3^{2+}$-AZM on Different Electrodes. The CV curve and ECL curve of the $Ru(bpy)_3^{2+}$-AZM system on a bare electrode, CNFs-1/GCE, and CNFs-2/GCE are shown in Figure 5. Compared with other electrodes, the oxidation peak current of the $Ru(bpy)_3^{2+}$-AZM system on the CNFs-2/GCE modified electrode is significantly higher, but the peak potential does not change (Figure 5(a)). In Figure 5(b), the ECL luminescence intensity of the $Ru(bpy)_3^{2+}$-AZM system is significantly improved on CNFs-2/GCE, which is about 35 times that of the bare electrode. It indicates that the CNFs-2 modified electrode pair $Ru(bpy)_3^{2+}$-AZM system has a significant sensitization effect, which may be because the larger specific surface area of CNFs-2 provides more reaction sites. The N in the tertiary amine group of AZM is oxidized to N cation radical. This radical is extremely unstable and will immediately undergo dehydrogenation reaction. A strongly reducing intermediate reduces $Ru(bpy)_3^{3+}$ to form an excited state $[Ru(bpy)_3^{2+}]*$. When the excited state returns to the ground state [24–26], it produces luminescence. The specific reaction process is as shown in formulas (1)–(5) as follows:

$$Ru(bpy)_3^{2+} - e^- \longrightarrow Ru(bpy)_3^{3+} \quad (1)$$

$$C_{38}H_{72}N_2O_{12} - e^- \longrightarrow C_{38}H_{72}N_2^{+} \cdot O_{12} \quad (2)$$

$$C_{38}H_{72}N_2^{+} \cdot O_{12} \longrightarrow C_{38}H_{72}N_2 \cdot O_{12} + H^+ \quad (3)$$

$$C_{38}H_{72}N_2 \cdot O_{12} + Ru(bpy)_3^{3+} \longrightarrow [Ru(bpy)_3^{2+}]* + \text{products} \quad (4)$$

$$[Ru(bpy)_3^{2+}]* \longrightarrow Ru(bpy)_3^{2+} + h\nu \quad (5)$$

3.3. Optimization of Detection Conditions. The modification amount of CNFs-2 on the electrode surface, the choice of buffer system, the size of pH, the choice of $Ru(bpy)_3^{2+}$ concentration, and instrument parameters will all affect the detection signal. So it needs to be optimized to obtain ECL signal with low background and high sensitivity.

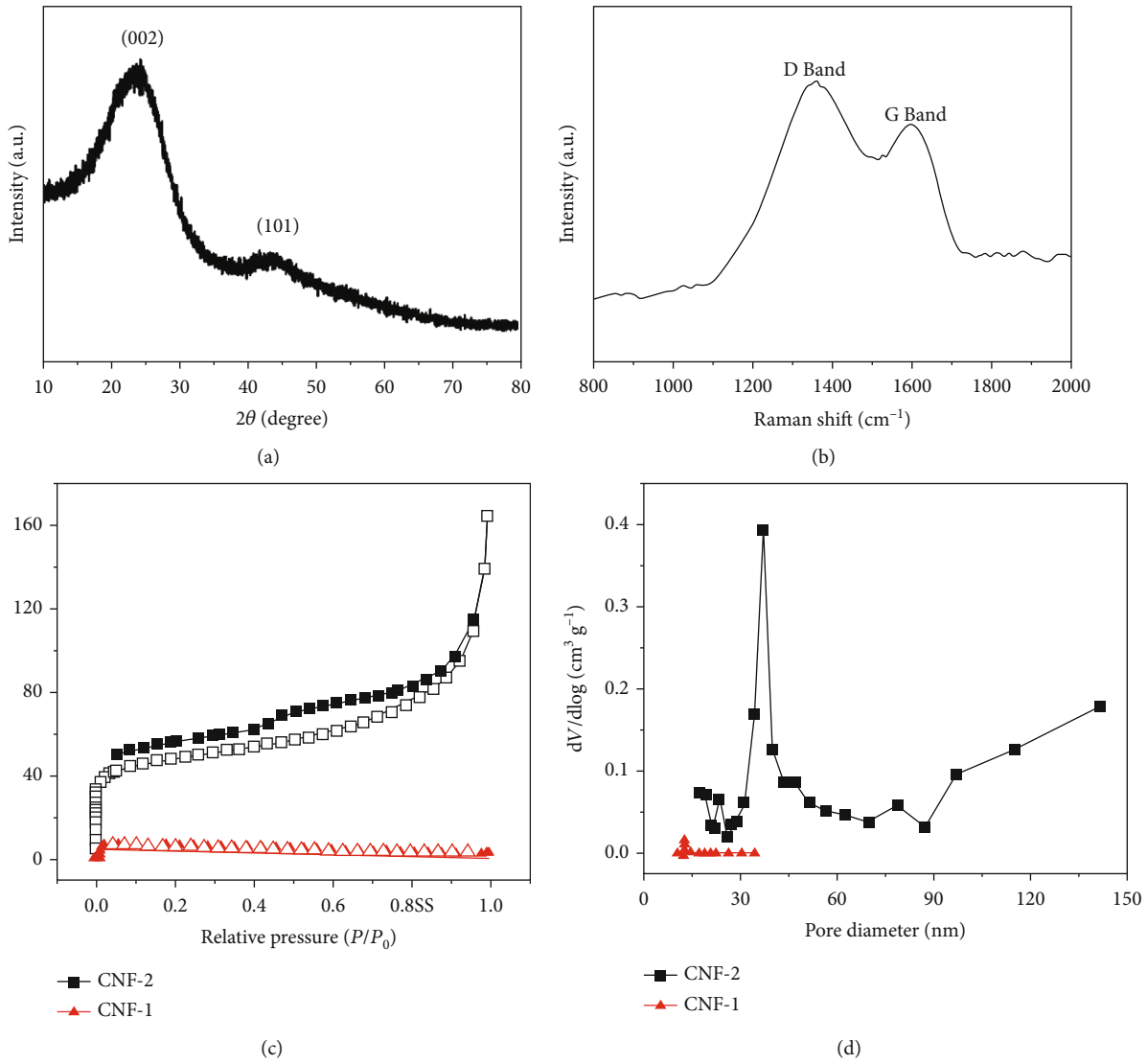

Figure 3: XRD pattern (a), Raman spectrum (b) of CNFs-2, N_2 adsorption-desorption isotherms (c), and pore size distribution curve (d) of the CNFs-1 and CNFs-2.

3.3.1. Effects of CNFs-2 Modification. The modification amount of CNFs-2 on the electrode surface is an important factor affecting the intensity of ECL. Figure6(a) investigates the influence of different modification amounts on the luminescence intensity of the $Ru(bpy)_3^{2+}$-AZM system. As shown in Figure 6(a), the ECL intensity increases with the increase of the modification amount. When the modification amount is 3 μL, the ECL intensity reaches the highest, and when the modification amount continues to increase, the luminescence intensity decreases instead [27–29]. Therefore, 3 μL is the best choice modification amount.

3.3.2. Effects of Buffer Type and pH Value. In order to investigate the influence of buffer solution and pH value on the luminescence intensity of the $Ru(bpy)_3^{2+}$-AZM system, the experiment investigated the changes of ECL intensity in phosphate buffer solution and borate buffer solution. The results are shown in Figure6(b). It can be seen that the luminescence intensity of the $Ru(bpy)_3^{2+}$-AZM system in phosphate buffer solution is significantly higher than that in borate buffer solution. When the pH is 8.5, the luminescence intensity reaches the highest and the signal-to-noise ratio is the largest. Moreover, the reproducibility is better. Thus, a phosphate buffer with a pH of 8.5 was chosen as the experimental buffer system.

3.3.3. Effects of the Concentration of $Ru(bpy)_3^{2+}$. The experiment investigated the influence of different $Ru(bpy)_3^{2+}$ concentrations on the ECL intensity. The results showed that the ECL signal of the $Ru(bpy)_3^{2+}$-AZM system increased with the increase of the luminescent substance concentration. When the concentration reached 1.0×10^{-4} mol·L^{-1}, the signal-to-noise ratio reaches the maximum. Further, increasing the concentration of $Ru(bpy)_3^{2+}$, the effect of increasing the luminous intensity is not obvious. In view of the expensive price of $Ru(bpy)_3^{2+}$, we select 1.0×10^{-4} mol·L^{-1} as the best concentration.

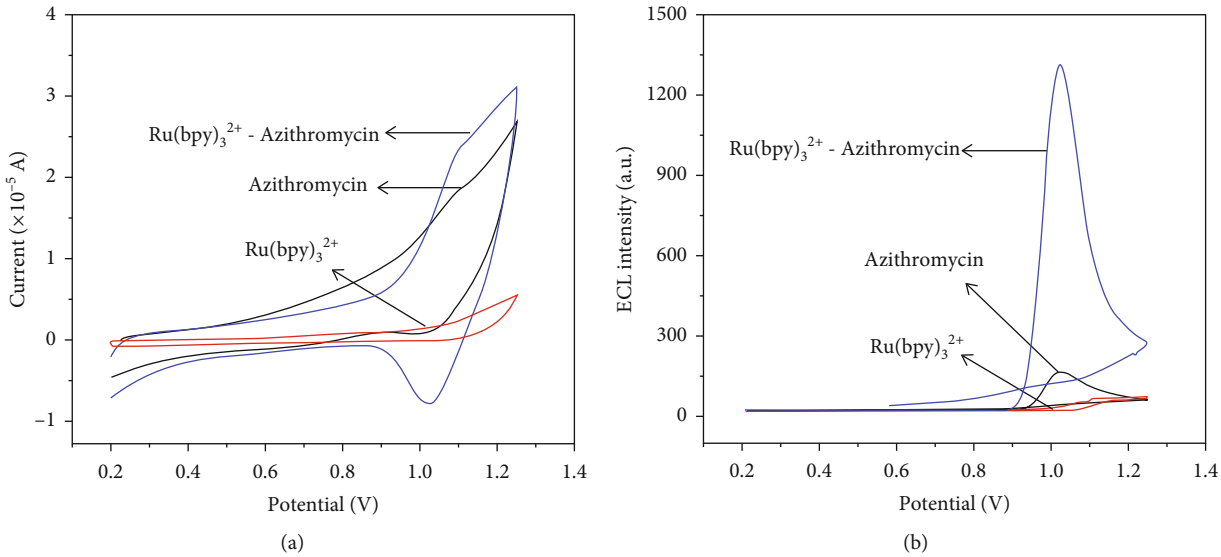

Figure 4: EC (a) and (b) the ECL curves of Ru(bpy)$_3^{2+}$, AZM, and Ru(bpy)$_3^{2+}$-AZM.

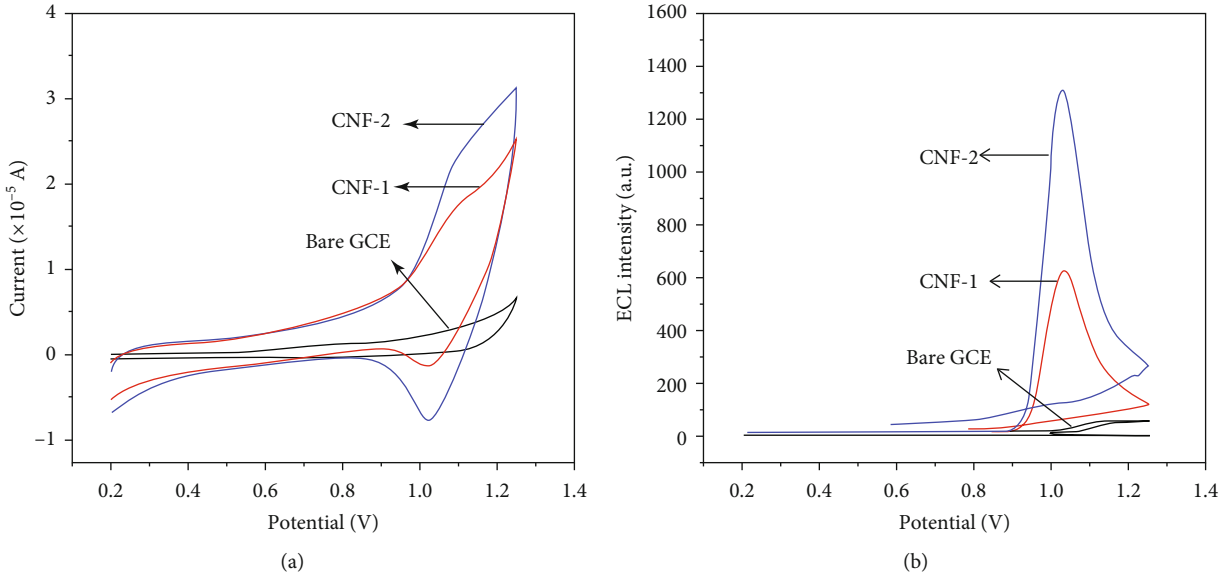

Figure 5: EC (a) and ECL (b) curves of Ru(bpy)$_3^{2+}$-AZM on different electrodes.

3.3.4. Selection of Instrument Parameters. The stability and sensitivity of the instrument detection will be affected by the negative high voltage value of the photomultiplier tube and the scanning speed. Therefore, the experimental study of the Ru(bpy)$_3^{2+}$-AZM system under the negative high voltage of -600 V to -900Vchanges in the luminous intensity. It is found that under the negative high voltage value of -800 V, the ECL strength is high and stable. At the same time, the experiment also investigated the influence of scanning speed in the range of 0.06-0.14 V·s^{-1} on the luminous intensity of the system. The results show that when the scanning speed is 0.10 V·s^{-1}, the luminous intensity of the system no longer increases. To get better stability and sensitivity, the experiment chooses -800 V negative high voltage and 0.10 V·s^{-1} as the best conditions.

3.4. Analytical Performance of the CNFs-2. Using the optimal conditions stated above, the variation of ECL intensity with AZM concentration was studied, and the results are shown in Figure 7. It can be seen from Figure 7(a) that the ECL intensity increases with the increase of the AZM concentration. The linear regression analysis of the AZM concentration by the ECL intensity shows that the AZM concentration is within the range of 8.0×10^{-8}-1.0×10^{-4} mol·L^{-1}. It shows a good linear relationship with ECL intensity (Figure 7(b)). The linear corresponding equation is $y = 175.83x + 8.49$ ($R^2 = 0.999$), and the limit of detection (LOD) was calculated about 6.52×10^{-8} mol·L^{-1} ($S/N = 3$). It can be seen from Table 1 that the method for detecting AZM established in this experiment has a lower detection limit and a wider linear range than other methods.

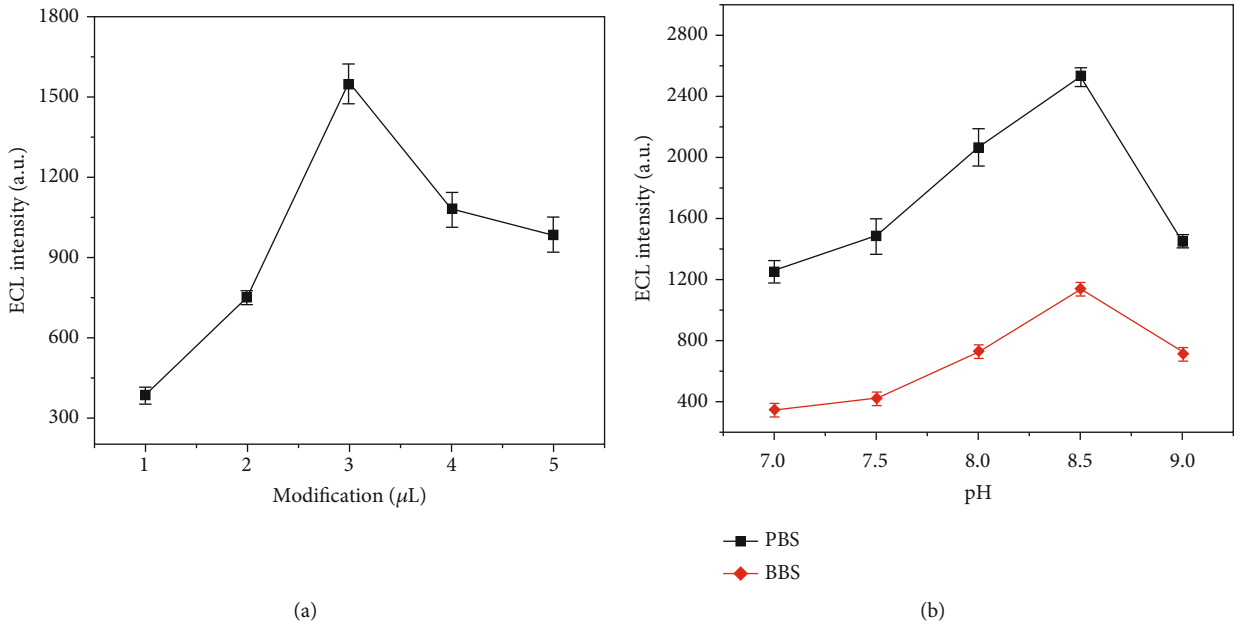

Figure 6: (a) Volume of CNF-2; (b) buffer type and pH value ($n = 3$).

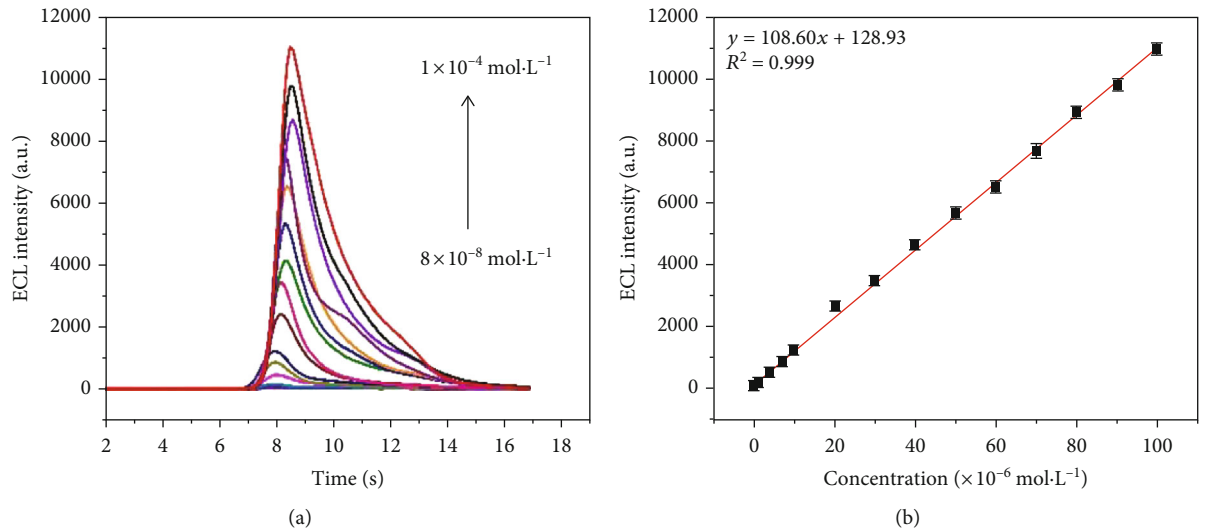

Figure 7: Under optimal conditions, the ECL responses at CNFs-2/GCE (a) and the calibration curves (b) of the different concentrations of AZM ($n = 3$).

3.5. Selectivity of the Sensor. Using the optimal conditions stated above, the selectivity of the modified electrode for AZM detection in the presence of other interfering substances was investigated, and the results are shown in Figure 8. It can be seen from the figure that 600-fold of Na^+, Cl^-, and K^+; 300 times of NH_4^+ and NO_3^-; 200-fold of Ca^{2+} and Mg^{2+}; 20-fold of glucose and fructose; and 5-fold of sucrose have no obvious interference on the detection of 1.0×10^{-5} mol·L^{-1} AZM. It indicates that the modified electrode has good selectivity.

3.6. Reproducibility and Repeatability of the Modified Electrodes. Using the same method to prepare 5 identical modified electrodes for ECL detection of AZM, the relative standard deviation (RSD) of the result was 3.07%. The repeatability inspection used the same modified electrode to detect AZM for 10 times, and the RSD was 2.36%. The results show that CNFs-2/GCE has good reproducibility and repeatability.

3.7. Analysis of a Real Sample. 10 AZM tablets were weighed and ground. Then, the collected powder was dissolved with 2% acetic acid by ultrasonic and prepared into 1.0×10^{-5} mol·L^{-1} solution. The ECL measurement was repeated 5 times under the optimal conditions. And the RSD of the result was 3.68%. After adding standard products to the actual samples for the recovery rate experiment, the results are listed in Table 2, and the recovery rate is between 98.08% and 101.76%, indicating that the method established

Table 1: Comparison of different methods used for the detection of AZM.

Methods	Linear range (mol/L)	LOD (mol/L)	References
Electrochemistry	1.33×10^{-8}-6.67×10^{-5}	8.5×10^{-9}	[6]
HPLC	1.34×10^{-4}–1.34×10^{-3}	—	[3]
LC-MS/MS	4.45×10^{-9}–1.11×10^{-6}	—	[5]
UV spectrophotometry	2.14×10^{-5}-1.29×10^{-4}	—	[7]
Spectrophotometry	1.00×10^{-5}-7.00×10^{-5}	—	[4]
ECL	4.00×10^{-7}-2.00×10^{-4}	3.00×10^{-9}	[1]
ECL	8.00×10^{-8}-1.00×10^{-4}	6.52×10^{-8}	This work

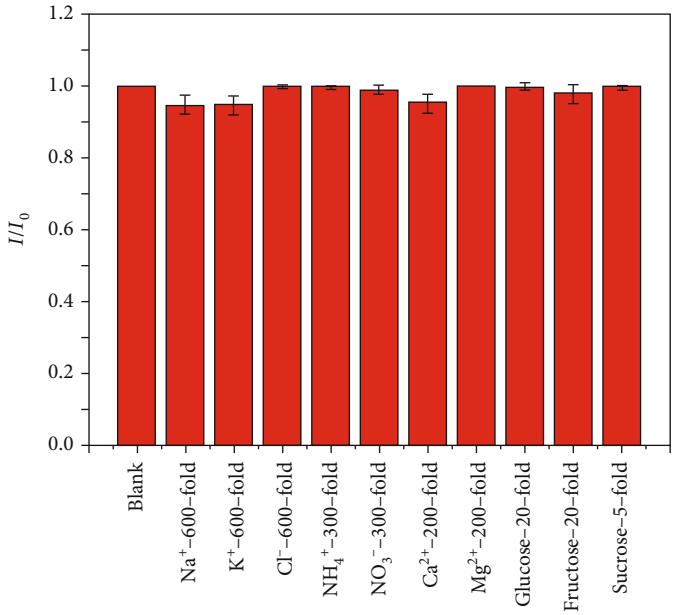

Figure 8: The interference study of CNFs-2/GCE for detecting AZM.

Table 2: Detection of AZM in real samples and their recoveries.

Sample ($\times 10^{-5}$ mol·L^{-1})	Added ($\times 10^{-5}$ mol·L^{-1})	Actual ($\times 10^{-5}$ mol·L^{-1})	Founded N ($\times 10^{-5}$ mol·L^{-1})	Recovery (%)	RSD (%, $n = 3$)
1.0	1.0	1.0	1.01 ± 0.03	100.06	1.28
	3.0	2.0	1.98 ± 0.01	98.08	3.25
	5.0	3.0	3.01 ± 0.02	100.48	4.49
	7.0	4.0	4.04 ± 0.18	101.76	2.67
	9.0	5.0	4.86 ± 0.08	98.43	3.00

in this paper can be used to determine the AZM in the actual sample.

4. Conclusions

In this study, high specific surface of CNFs-2 was prepared by the electrospinning method and a new method of ECL detection of AZM was established by modifying GCE. Under the optimal conditions, the EC behavior and ECL behavior of the $Ru(bpy)_3^{2+}$-AZM system on the modified electrode were investigated. The results show that the prepared material has good electrocatalytic activity for azithromycin and in the range of 8.0×10^{-8}-1.0×10^{-4} mol·L^{-1} and the concentration of AZM has a good linear relationship with the luminous intensity. The linear equation is $y = 175.83x + 8.49$ ($R^2 = 0.999$), and the LOD is 6.52×10^{-8} mol·L^{-1} ($S/N = 3$). This method can be used for the detection of actual samples.

Data Availability

The basic data for the experiment can be provided by the author.

Conflicts of Interest

The author(s) declare(s) that they have no conflicts of interest.

Acknowledgments

This work was financially supported by the National Natural Science Foundation of China (Grant No. 21968005), the

Natural Science Foundation of Shandong (Grant No. ZR2019MB039), Innovation Project of Guangxi Graduate Education (No. YCSW2019208), Innovation Project of Guangxi University of Science and Technology Graduate Education (No. GKYC202127), and the High Levels of Innovation Team and Excellence Scholars Program in colleges of Guangxi.

References

[1] S. D. Patil, T. Dugaje, and S. J. Kshirsagar, "Development and validation of UV spectrophotometric method for estimation of cyproheptadine hydrochloride," *Asian Journal of Research in Chemistry*, vol. 12, no. 2, pp. 112–115, 2019.

[2] R. Abdel-Hamid and E. F. Newair, "Voltammetric determination of ferulic acid using polypyrrole-multiwalled carbon nanotubes modified electrode with sample application," *Nanomaterials*, vol. 5, no. 4, pp. 1704–1715, 2015.

[3] S. L. Merhar, S. P. Pentiuk, V. A. Mukkada, J. Meinzen-Derr, A. Kaul, and D. R. Butler, "A retrospective review of cyproheptadine for feeding intolerance in children less than three years of age: effects and side effects," *Acta Paediatrica*, vol. 105, no. 8, pp. 967–970, 2016.

[4] M. Guo, L. Sun, L. Liu, S. Song, H. Kuang, and G. Cui, "Ultrasensitive immunochromatographic strip for detection of cyproheptadine," *Food and Agricultural Immunology*, vol. 29, no. 1, pp. 941–952, 2018.

[5] J. Yang, Z. Wang, T. Zhou et al., "Determination of cyproheptadine in feeds using molecularly imprinted solid- phase extraction coupled with HPLC," *Journal of Chromatography B-analytical Technologies in the Biomedical and life sciences*, vol. 990, pp. 39–44, 2015.

[6] X. Feás, L. Ye, S. V. Hosseini, C. A. Fente, and A. Cepeda, "Development and validation of LC-MS/MS method for the determination of cyproheptadine in several pharmaceutical syrup formulations," *Journal of Pharmaceutical and Biomedical Analysis*, vol. 50, no. 5, pp. 1044–1049, 2009.

[7] D. Zhu, X. Li, J. Sun, and T. You, "Chemometrics optimization of six antihistamines separations by capillary electrophoresis with electrochemiluminescence detection," *Talanta*, vol. 88, pp. 265–271, 2012.

[8] C. Hasegawa, T. Kumazawa, X. P. Lee et al., "Simultaneous determination of ten antihistamine drugs in human plasma using pipette tip solid-phase extraction and gas chromatography/mass spectrometry," *Rapid Communications in Mass Spectrometry*, vol. 20, no. 4, pp. 537–543, 2006.

[9] L. L. Yang, L.-J. Li, Y. Luo et al., "Preparation of electrochemiluminescence sensor by immobilizing tris(2,2′-bipyridine)ruthenium (II) on gold electrode with nanoTiO_2-ZnO/silica sol/conductive adhesive composite film," *Chinese Journal of Analytical Chemistry*, vol. 43, no. 4, pp. 547–552, 2015.

[10] J. Sun, W. Gao, L. Qi et al., "Detection of 1,3-dihydroxyacetone by tris(2,20 -bipyridine)ru.Zhang, Y.; Lv, J.-R. Determination of diphenidol hydrochloride by post-chemiluminescence reaction," *Journal of Analytical Science*, vol. 410, pp. 2315–2320, 2018.

[11] Y. Wu, X. Li, X. Tan et al., "A cyclic catalysis enhanced electrochemiluminescence aptasensor based 3D graphene/photocatalysts Cu_2O-MWCNTs," *Electrochimica Acta*, vol. 282, pp. 672–679, 2018.

[12] J. Hu, C. Zhai, and M. Zhu, "Photo-responsive metal/semiconductor hybrid nanostructure: a promising electrocatalyst for solar light enhanced fuel cell reaction," *Chinese Chemical Letters*, vol. 32, no. 4, pp. 1348–1358, 2021.

[13] S. Hu, Y. Yu, Y. Guan, Y. Li, B. Wang, and M. Zhu, "Two-dimensional TiO2 (001) nanosheets as an effective photo-assisted recyclable sensor for the electrochemical detection of bisphenol A," *Chinese Chemical Letters*, vol. 31, no. 10, pp. 2839–2842, 2020.

[14] Z. Li and M. Zhu, "Detection of pollutants in water bodies: electrochemical detection or photo-electrochem," *Chemical Communications*, vol. 56, no. 93, pp. 14541–14552, 2020.

[15] Q. Xue, J. Sun, Y. Huang et al., "Recent progress on flexible and wearable supercapacitors," *Small*, vol. 13, no. 45, p. 1701827, 2017.

[16] Q. Wang, Y. Ji, Y. Lei et al., "Pyridinic-N-dominated doped defective graphene as a superior oxygen electrocatalyst for ultrahigh-energy-density Zn-air batteries," *ACS Energy Letters*, vol. 3, no. 5, pp. 1183–1191, 2018.

[17] C. Lv, C. Yan, G. Chen et al., "An amorphous noble-metal-free electrocatalyst that enables nitrogen fixation under ambient conditions," *Angewandte Chemie International Edition*, vol. 57, no. 21, pp. 6073–6076, 2018.

[18] Z. Li, H. Zhang, and M. Zhu, "Photo-electrochemical detection of dopamine in human urine and calf serum based on MIL-101 (Cr)/carbon black," *Microchimica Acta*, vol. 187, p. 526, 2020.

[19] X. Wang, H. Gao, C. Zhai, Z. He, C. Yuan, and M. Zhu, "Newly found photoactivated Pt anchored on three-dimensional layered WS2/carbon cloth for highly efficient ethylene glycol electro-oxidation," *Industrial & Engineering Chemistry Research*, vol. 59, no. 43, pp. 19252–19259, 2020.

[20] Y. Xiao, Y. Xu, K. Zhang et al., "Coaxial electrospun free-standing and mechanically stable hierarchical porous carbon nanofiber membranes for flexible supercapacitors," *Carbon*, vol. 160, pp. 80–87, 2020.

[21] Z. He, Y. Jiang, J. Zhu et al., "N-doped carbon coated $LiTi_2(PO_4)_3$ as superior anode using PANi as carbon and nitrogen bi-sources for aqueous lithium ion battery," *Electrochimica Acta*, vol. 279, pp. 279–288, 2018.

[22] H. He, Q. Gan, H. Wang et al., "Structure-dependent performance of TiO_2/C as anode material for Na-ion batteries," *Nano Energy*, vol. 44, pp. 217–227, 2018.

[23] T. H. Fereja, S. A. Kitte, D. Snizhko et al., "Tris(2,2′-bipyridyl)ruthenium(II) electrochemiluminescent determination of ethyl formate," *Analytical and Bioanalytical Chemistry*, vol. 410, no. 26, pp. 6779–6785, 2018.

[24] H. Cheng, Z. Zhou, Y. Li et al., "Electrochemiluminescence sensor based on electrospun three-dimensional carbon nanofibers for the detection of difenidol hydrochloride," *Sensors*, vol. 19, no. 15, pp. 3315–3327, 2019.

[25] H. Cheng, Z. Zhou, and T. Liu, "Electro-spinning fabrication of nitrogen, phosphorus co-doped porous carbon nanofiber as an electro-chemiluminescent sensor for the determination of cyproheptadine," *RSC Advances*, vol. 10, no. 39, pp. 23091–23096, 2020.

[26] H. Cheng, Z. Zhou, D. Qin et al., "Electrochemical sensor based on electrospun three-dimensional carbon nanofibers to determine trace levels of Cu(II)," *Science of Advanced Materials*, vol. 12, no. 5, pp. 693–700, 2020.

[27] H. Wang, X. Huang, W. Li et al., "TiO_2 nanoparticle decorated carbon nanofibers for removal of organic dyes," *Colloids and*

Surfaces A: Physicochemical and Engineering Aspects, vol. 549, pp. 205–211, 2018.

[28] A. Vinu, S. Anandan, C. Anand, P. Srinivasu, K. Ariga, and T. Mori, "Fabrication of partially graphitic three-dimensional nitrogen-doped mesoporous carbon using polyaniline nanocomposite through nanotemplating method," *Microporous and Mesoporous Materials*, vol. 109, no. 1-3, pp. 398–404, 2008.

[29] H. Zhang, J. He, C. Zhai, and M. Zhu, "2D Bi_2WO_6/MoS_2 as a new photo-activated carrier for boosting electrocatalytic methanol oxidation with visible light illumination," *Chinese Chemical Letters*, vol. 30, no. 12, pp. 2338–2342, 2019.